Hindawi
International Journal of Antennas and Propagation
Volume 2023, Article ID 1633484, 8 pages
https://doi.org/10.1155/2023/1633484

Research Article

Practical Noise Model of an Active Electronically Scanning Array

Jian Mi, Kan Wang, Zhao Li, and Hongbing Sun

Nanjing Research Institute of Electronics Technology, Nanjing 210039, China

Correspondence should be addressed to Jian Mi; mijian@pku.edu.cn

Received 16 May 2022; Revised 27 December 2022; Accepted 7 January 2023; Published 16 January 2023

Academic Editor: Rajkishor Kumar

Active electronically scanning arrays are now widely used in radar and communication systems. The noise characteristics are critical to the system signal-to-noise ratio, thus modeling of the antenna array noise is useful. In this paper, a two-port noise model of an active electronically scanning array is presented, which is more practical than the model in previous publications. In this model, an antenna array with a multistage combiner network is equivalent to a one-stage combiner network, thus the calculation of the noise figure is greatly simplified. Since the model is based on measurable parameters, it can be applied directly to the design of electronically scanning arrays. The noise model of a spaceborne synthetic aperture radar antenna system is displayed for example. Some useful conclusions are got about the noise figure for tapered antenna arrays. For a weighted antenna array with taper efficiency ε_T, if the gain of low noise amplifiers is sufficiently large, the noise figure of the antenna array is increased by $1/\varepsilon_T$, compared to a uniformly weighted array. Besides, the deterioration of the signal-to-noise ratio for a tapered antenna array system originates from the increase of antenna noise temperature, rather than the decrease of antenna aperture gain.

1. Introduction

Active electronically scanning arrays (AESAs) with Transmit-Receive modules (TRMs) to control the amplitude and phase of each radiating element are widely used in radar and communication systems. They are capable of rapid beam steering and beamforming, making it possible to track multiple targets simultaneously. In addition, AESAs have higher reliability compared to conventional reflector antennas: the failure of some channels in the array will not lead to the failure of the antenna system.

In the receiving system, the signal-to-noise ratio (SNR) is mainly determined by the system noise characteristics, thus modeling of the system noise becomes a critical issue. For two-port components in AESAs such as TRM and time delay module (TDU), the noise parameter can be easily measured by noise measuring instruments. However, the noise characteristic evaluation of the system is not an easy task. The antenna array comprises multiple receiving channels with different amplitude and phase, and the noise figure varies with array weighting coefficients. Besides, the external noise temperature is not constant and is dependent on the antenna radiation pattern and spatial noise temperature distribution, resulting in a complicated noise model of the antenna array.

A basic system-level model for the gain and G/T of an active array antenna is presented in [1]. The noise temperature is referenced at the output terminal of the radiating antenna, that the antenna array is divided into two parts: passive radiating antenna array and active beamforming network. This model is still complicated because the antenna array cannot be regarded as a simple two-port component, which is convenient in calculating the SNR of receiving system. Subsequent publications continue to use the definition of reference point for noise temperature.

The computation of noise figure for an AESA has been studied by Lee [2] and Gatti et al. [3]; however, the method is based on a simple antenna array structure with only a one-stage beamforming network. In practical applications, the active antenna array is more complicated with a multistage combiner network, and the formulas in [3] are not applicable. Optimization of the subarray structure to improve the G/T of an antenna array is shown in [4] by Yun, and the calculation of the noise figure for an antenna array is displayed in detail. But the calculation process is very complicated for the multistage beamforming network and is only

useful for the array structure in the reference. A simple, universal, and practical noise model is needed to simplify the noise figure calculation for multichannel AESAs. Holzman [5] raises a different perspective on taper efficiency for array antennas that reveals the relationship between taper efficiency and system SNR. Other applications of noise figures are shown in [6–8].

In this paper, an improved noise model for an AESA is proposed. The noise temperature is referenced at the input terminal of the radiating antenna and outside the ASEA system, so the antenna array could be equivalent to a simple two-port component with noise temperature T_a and signal gain G_a. The model is universal and practical. In the calculation of T_a, we deduce that an antenna array with a multistage combiner network is equivalent to a one-stage combiner network, making the calculation greatly simplified. Noise models for components such as radiating antenna, TRU, and TDU are also studied in this paper. Some useful conclusions are got about the noise figure for tapered antenna arrays. For a weighted antenna array with taper efficiency ε_T, if the gain of low noise amplifiers (LNAs) is sufficiently large, the noise figure of the antenna array is increased by $1/\varepsilon_T$ compared to a uniformly weighted array. Besides, the deterioration of the signal-to-noise ratio for a tapered antenna array system originates from the increase of antenna noise temperature, rather than the decrease of antenna aperture gain. The noise model is applied in a spaceborne AESA system, which shows the noise figure of AESA varies with Taylor weighting depth. This paper is a comprehensive description of the noise model for AESAs and will deepen the understanding on a system with multiple receiving channels.

2. Noise Model of an AESA

2.1. System-Level Model. A system-level noise model of an AESA is shown in Figure 1. The antenna array is equivalent to a two-port component with noise temperature T_a and signal gain G_a. S_i and T_{ext} are the input signal power and external noise temperature. T_{rec} is the noise temperature of the receiver.

G_a differs from the antenna pattern gain G_p, which is proportional to its effective aperture A_e:

$$G_p = \frac{4\pi A_e}{\lambda^2}\varepsilon_T, \tag{1}$$

where λ is the wavelength and ε_T is the taper efficiency of the antenna which characterizes the gain loss of a weighted antenna array. A_e is not constant but varies with antenna beam steering angle θ:

$$A_e = A_0 \cos\theta. \tag{2}$$

A_0 is the aperture area of the antenna. For an AESA, ε_T is defined as follows [9]:

$$\varepsilon_T = \frac{\left|\sum_{i=1}^{n} a_i\right|^2}{n\sum_{i=1}^{n}\left|a_i\right|^2}, \tag{3}$$

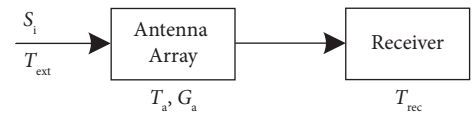

Figure 1: System-level model for receiving system.

where a_i is the complex weighting coefficient of the i th channel and n is the number of channels of an AESA.

When a plane wave with power density p_{in} comes into an antenna array with effective aperture A_e, the input signal power S_i is determined as

$$S_i = p_{in} A_e. \tag{4}$$

The external noise temperature T_{ext} is as follows [5]:

$$T_{ext} = \frac{\int_0^{2\pi}\int_0^{2\pi} T_B(\theta,\phi) D(\theta,\phi)\sin\theta d\theta\, d\phi}{\int_0^{2\pi}\int_0^{2\pi} D(\theta,\phi)\sin\theta d\theta\, d\phi}, \tag{5}$$

where $T_B(\theta, \phi)$ is the brightness temperature distribution of all external noise source and $D(\theta, \phi)$ is the antenna array directivity pattern. But if the bandwidth is very large, the noise is noncoherent, this case is discussed in [1]. The external noise is complicated and varies with the external environment, antenna array pattern, and system bandwidth.

The noise temperature T_{sys} and SNR of the receiving system is given by the following equation:

$$T_{sys} = T_{ext} + T_a + \frac{T_{rec}}{G_a}, \tag{6}$$

$$\begin{aligned} \mathrm{SNR} &= \frac{S_i}{N_{sys}} \\ &= \frac{p_{in}}{kB}\frac{A_e}{T_{sys}}. \end{aligned} \tag{7}$$

Here, k is Boltzmann constant and B is the system bandwidth. The antenna noise temperature is $T_a = (F_a - 1)T_0$, where T_0 (290 K) is the reference temperature and F_a is the antenna noise figure. The aim of this paper is to calculate T_a and G_a for the antenna system.

2.2. Noise Figure Calculation for an AESA. Figure 2 shows a typical block diagram of an AESA. The beamforming network is composed of a 3-stage combiner network (M:1 combiners, N:1 combiners, a P:1 combiner), Transmit-Receive modules (TRM), and time delay modules (TDU). M radiating antennas are connected to a TRM to realize signal amplification with low noise and the control of phase and amplitude for each channel. N TRMs are connected to a TDU unit to compensate for time delay when beam steering. P TDUs are combined to form the received signal.

To calculate the noise temperature or noise figure of the antenna array, we first study a lossless combiner network shown in Figure 3. The noise figure and power gain of the i th branch are NF_i and G_i,

$$G_i = \left|a_i\right|^2, \tag{8}$$

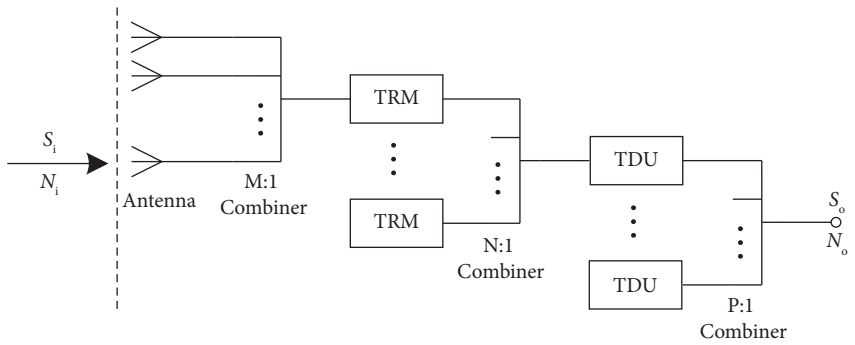

Figure 2: Block diagram of an AESA.

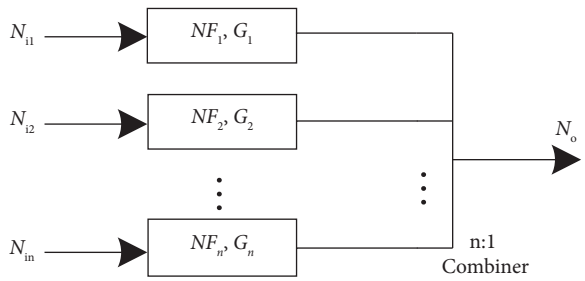

Figure 3: Noise model of a combiner network.

where a_i is the voltage gain, which contains amplitude and phase change in each branch. Assume that the input noise temperature of each branch is T_0, thus

$$\begin{aligned} N_{i1} &= N_{i2} \\ &= \cdots \\ &= N_{\text{in}} \\ &= kT_0B. \end{aligned} \tag{9}$$

The output noise power is

$$\begin{aligned} N_{\text{o}} &= \sum_{i=1}^{n} \frac{N_{\text{o}i}}{n} \\ &= \sum_{i=1}^{n} \frac{kT_0BG_iNF_i}{n} \\ &= \frac{kT_0B}{n} \sum_{i=1}^{n} G_iNF_i. \end{aligned} \tag{10}$$

From the scattering matrix of a $n:1$ combiner [9, 10], the signal power gain of the combiner network is

$$\begin{aligned} G_{\text{sign}} &= \frac{\left|\left(\sum a_i/\sqrt{n}\right)\right|^2}{n} \\ &= \frac{\left|\sum_{i=1}^{n} a_i\right|^2}{n^2}. \end{aligned} \tag{11}$$

We can get the noise figure of the network

$$\begin{aligned} NF &= \frac{(S_{\text{in}}/N_{\text{in}})}{(S_{\text{o}}/N_{\text{o}})} \\ &= \frac{N_{\text{o}}}{N_{\text{in}}G_{\text{sign}}} \\ &= n\frac{\left(\sum_{i=1}^{n} G_iNF_i\right)}{\left|\sum_{i=1}^{n} a_i\right|^2}. \end{aligned} \tag{12}$$

For a more complicated combiner network is shown in Figure 4(a), the combiner is connected to a module with noise figure F_1 and signal power gain H_1, where $H_1 = |h_1|^2$. Noise figure and gain of the left part is the same as equations (11) and (12), thus the total noise figure and signal gain are obtained.

$$\begin{aligned} NF_{\text{a}} &= NF_{\text{left}} + \frac{F_1 - 1}{G_{\text{sign\_left}}} \\ &= \frac{n\sum_{i=1}^{n} G_i\left[NF_i + \left((F_1 - 1)/G_i\right)\right]}{\left|\sum_{i=1}^{n} a_i\right|^2}, \\ G_{\text{sign\_a}} &= G_{\text{left}}H_1 \\ &= \frac{\left|\sum_{i=1}^{n} a_ih_1\right|^2}{n^2}. \end{aligned} \tag{13}$$

In Figure 4(b), the module is assigned to each branch of the combiner network, and the noise figure and signal gain of the i th branch are

$$\begin{aligned} NF_{bi} &= NF_i + \frac{(F_1 - 1)}{G_i}, \\ G_{\text{b}i} &= G_iH_1 \\ &= \left|a_ih_1\right|^2. \end{aligned} \tag{14}$$

The noise temperature and gain for Figure 4(b) are

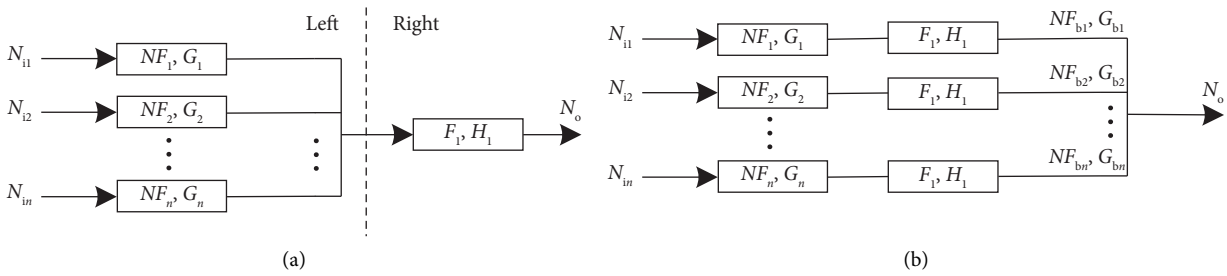

Figure 4: Noise model of a combiner network.

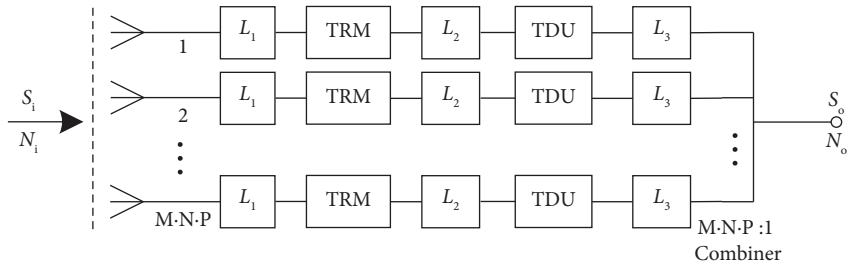

Figure 5: Block diagram of a one-stage combiner network.

$$NF_b = \frac{n\sum_{i=1}^{n} G_{bi}NF_{bi}}{\left|\sum_{i=1}^{n} a_i h_1\right|^2} = \frac{n\sum_{i=1}^{n} G_i\left[NF_i + \left((F_1 - 1)/G_i\right)\right]}{\left|\sum_{i=1}^{n} a_i\right|^2}, \quad (15)$$

$$G_{\text{sign\_b}} = \frac{\left|\sum_{i=1}^{n} a_i h_1\right|^2}{n^2}.$$

It is obvious that $NF_a = NF_b$, $G_{\text{sign\_a}} = G_{\text{sign\_b}}$. We can conclude that Figure 4(a) and 4(b) are equivalent for the calculation of noise characteristics.

For a multistage combiner network in Figure 2, a module at the output port of a combiner can be assigned to each branch of the combiner, including the common loss of the combiner network. Thus, Figure 2 is equivalent to a one-stage combiner network shown in Figure 5. L_1, L_2, and L_3 are the equivalent loss of the network. Each branch is connected to a lossless M•N•P:1 combiner. It is easy to get the signal gain G_i and noise figure NF_i of the i th branch by cascaded noise equation [10] and calculate the gain G_a and noise figure F_a of the AESA by equations (11) and (12).

2.3. Noise Model of Components in AESA. Each branch of the antenna array is composed of radiating antenna, T/R module, time delay module, and loss between components. In this section, we will study the noise model of these components.

2.3.1. Radiating Antenna. The noise figure of a receiving antenna is discussed by Best [11]. The antenna is a one-port element and the noise temperature is referenced at the output terminal of the antenna. We consider a two-port antenna model as shown in Figure 6(a). The antenna is characterized by radiation efficiency η and match coefficient τ which is associated with standing-wave ratio ($\eta \le 1$, $\tau \le 1$). The antenna is connected to a component with gain G_e and noise temperature T_e. Assume that the input noise power is kT_0B, the output signal power and noise power is

$$S_o = \tau\eta G_e S_i,$$
$$N_o = \left[\tau\eta kT_0B + \tau(1-\eta)kT_pB\right]G_e + kT_eBG_e. \quad (16)$$

Here, T_p is the physical temperature of the antenna. The noise figure and noise temperature of the system is

$$F_{\text{radi}} = \frac{S_i}{N_i}\cdot\frac{N_o}{S_o} = 1 + \left(\frac{1}{\eta} - 1\right)\frac{T_p}{T_0} + \frac{1}{\eta\tau}\frac{T_e}{T_0},$$
$$T_{\text{radi}} = (F_{\text{radi}} - 1)T_0 = \left(\frac{1}{\eta} - 1\right)T_p + \frac{(T_e/\tau)}{\eta}. \quad (17)$$

This receiving system is equivalent to an attenuator with loss $L = 1/\eta$ connected to a component with noise temperature T_e/τ as shown in Figure 6(b). The mismatch increases the noise temperature after the output terminal of the antenna. In most cases, $T_p = T_0$, but in some ultralow noise receiving system such as radio telescopes, the antenna is immersed in a refrigerator, and T_p is much smaller than T_0.

2.3.2. T/R Module. The diagram of the receiving chain for a typical T/R module is displayed in Figure 7(a). It is consisted of circulator, low noise amplifier (LNA), phased shifter, and

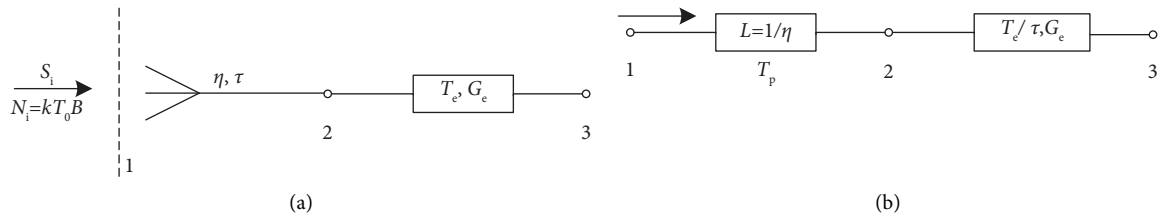

Figure 6: Noise model of radiating antenna.

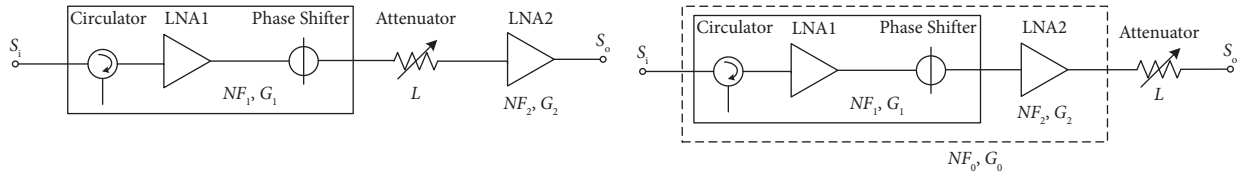

Figure 7: Block diagram of T/R module.

variable attenuator. The array weighting is realized by phase and amplitude control. Amplitude control will influence the noise figure and gain of the T/R module. There exists an output amplifier LNA2 after the attenuator. This model can be equivalent to a phase-control- only T/R module connected to an attenuator shown in Figure 7(b) for simplification. The noise figures of the two models are

$$\begin{aligned} F_{\text{TR\_a}} &= NF_1 + \frac{L-1}{G_1} + \frac{NF_2 - 1}{(G_1/L)} \\ &= NF_1 + \frac{NF_2 \cdot L - 1}{G_1}, \\ F_{\text{TR\_b}} &= NF_1 + \frac{NF_2 - 1}{G_1} + \frac{L-1}{G_1 G_2}. \end{aligned} \tag{18}$$

The noise figure difference is

$$F_{\text{TR\_a}} - F_{\text{TR}_b} = \frac{L-1}{G_1}\left(NF_2 - \frac{1}{G_2}\right). \tag{19}$$

In the case of $L << G_1$, we can get $F_{\text{TR\_a}} \approx F_{\text{TR\_b}}$, thus the model simplification is appropriate. The noise figure NF_0 is often obtained by the Y-factor method [12, 13], which is carried out by employing a noise analyzer.

2.3.3. Time Delay Module. The time delay module is composed of amplifiers and time delay lines. The delay line length is digitally adjustable by switches. The gain and phase of each delay line state are designed to keep nearly constant, thus the noise figure of the module remains unchanged. The noise figure is also measured by the Y-factor method.

2.4. Discussion on System SNR. For each branch is shown in Figure 5, if the gain of the first stage LNA in the T/R module is sufficiently large, together with a low amplitude weight, the noise figure of each branch will have no significant change when array weighting. Besides, all the branches show the high amplitude and phase consistency, we can obtain the following equation:

$$\begin{aligned} NF_1 &= NF_2 \\ &= \cdots \\ &= NF_n. \end{aligned} \tag{20}$$

From equation (12), the noise figure of the antenna array is

$$\begin{aligned} F_{\text{a}} &= nNF_1\left(\frac{\sum_{i=1}^{n} |a_i|^2}{\left|\sum_{i=1}^{n} a_i\right|^2}\right) \\ &= \frac{NF_1}{\varepsilon_T}, \end{aligned} \tag{21}$$

where ε_T is the taper efficiency of the weighted array in equation (3). The noise figure of the antenna array is increased by $1/\varepsilon_T$, compared to a uniformly weighted array. This result is consistent with reference [5], in which the taper efficiency is equal to the SNR of the weighted beamformer divided by the SNR of the uniformly weighted beamformer.

The system SNR is described by equations (6) and (7). For a special case, if the external noise temperature is assumed to be T_0, and the antenna gain G_{a} is sufficiently large, the noise temperature of the system is obtained as

$$T_{\text{sys}} \approx T_0 + (F_{\text{a}} - 1)T_0 = T_0 \cdot \left(\frac{NF_1}{\varepsilon_T}\right). \tag{22}$$

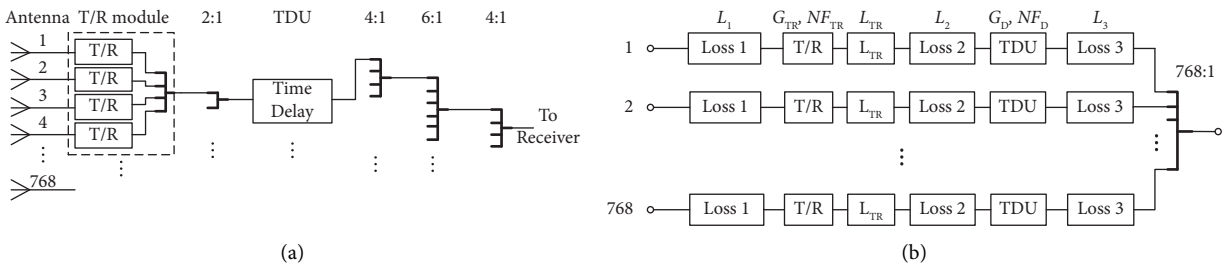

Figure 8: (a) Block diagram of GF-3 SAR antenna. (b) The noise model for the SAR antenna.

Table 1: Parameters of the noise model for GF-3 SAR antenna.

Parameter	Value (dB)
G_{TR}	32.1 ± 0.6
G_D	13.8 ± 0.4
L_2	0.21
NF_{TR}	2.35 ± 0.15
NF_D	2.43 ± 0.25
L_3	15.5

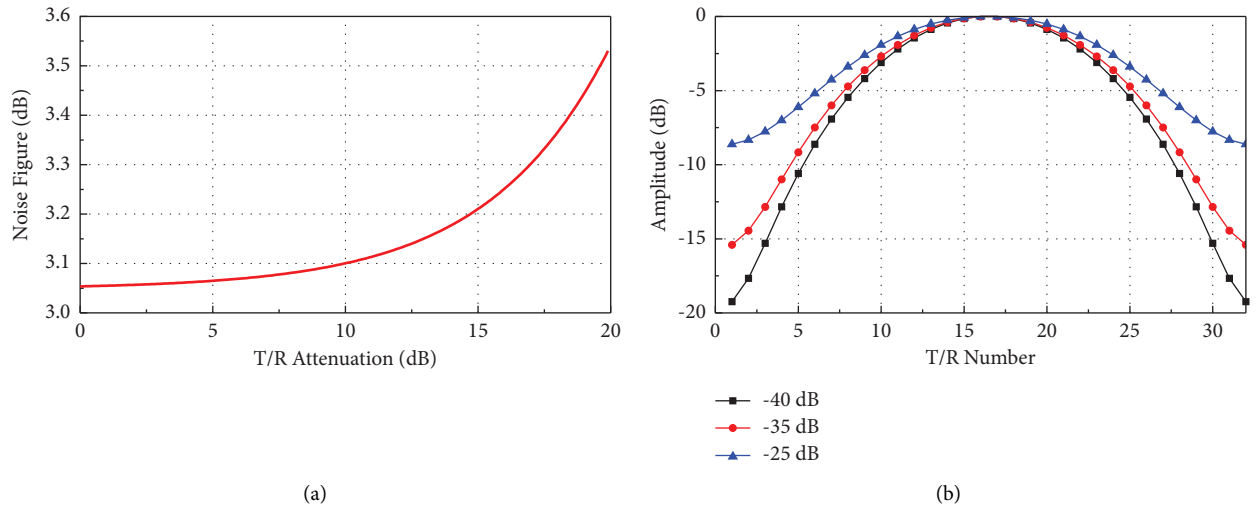

Figure 9: (a) Noise figure of each branch versus T/R attenuation. (b) T/R module weighting coefficient in the elevation direction.

Table 2: Antenna noise figure results for Taylor weighting.

SLL level (dB)	−20	−25	−30	−35	−40
F_a (dB)	3.272	3.492	3.750	3.977	4.214
ε_T	0.952	0.905	0.853	0.810	0.767
NF_0 / ε_T (dB)	3.269	3.488	3.745	3.971	4.207

The signal-to-noise ratio is

$$\begin{aligned} \mathrm{SNR} &= \frac{p_{\mathrm{in}} A_e \varepsilon_T}{kBT_0 NF_1} \\ &= \frac{p_{\mathrm{in}} \lambda^2}{4\pi kBT_0 NF_1} \frac{4\pi A_e \varepsilon_T}{\lambda^2} \\ &= \frac{p_{\mathrm{in}} \lambda^2 G_p}{4\pi kBT_0 NF_1}. \end{aligned} \tag{23}$$

Here, G_p is the antenna pattern gain of a weighted array. When the AESA is weighted, the deterioration of SNR for a receiving system originates from the increase of antenna noise temperature, rather than the decrease of antenna aperture gain. The input signal power keeps constant because the aperture area is unchanged. On the other hand, it is equivalent that the antenna noise remains constant but the antenna aperture gain G_p decreases.

G/T is often used to characterize the system SNR. In our noise model, the antenna noise temperature is referenced at the input terminal of the radiating antenna, thus G will not

change when array weighting. We only need to consider the noise temperature of the receiving system.

3. Application Example

To illustrate the applicability of the noise figure calculation method, consider for example the design of an SAR antenna for a GF-3 satellite. GF-3 is the first C-band multi-polarization SAR satellite in China and successfully launched in 2016 and 2021 [14–17]. For each polarization, the antenna is made of 768 slot waveguide antennas (24 in azimuth direction and 32 in elevation direction), 192 4-channel T/R modules, 96 time delay modules, and combiner networks. The block diagram of the antenna is displayed in Figure 8(a).

In the calculation of noise figure, the multistage combiner network is simplified as a one-stage combiner network, which is shown in Figure 8(b). The parameter of the waveguide antenna is: $\eta = 0.9$, $\tau = 0.95$ (VSWR < 1.6), and $T_p = T_0$. The antenna is matched well so that the influence of τ can be ignored, and the antenna is equivalent to a 0.4 dB attenuator. Besides, the loss between the antenna and TDU is 0.3 dB, thus $L_1 = 0.7$ dB. L_{TR} is the variable attenuator used for array weighting. The value of other parameters is listed in Table 1. G_{TR} and G_D are the signal gain of the T/R module and TDU. NF_{TR} and NF_D are the noise figure of the T/R module and TDU. L_2 is the loss between the T/R module and TDU, and L_3 is the loss between TDU and the receiver.

For the i th branch, the noise figure is as follows [5]:

$$NF_i = L_1 + \frac{NF_{TR} - 1}{(1/L_1)} + \frac{L_{TR\_i}L_2 - 1}{(G_{TR}/L_1)} + \frac{NF_D - 1}{G_{TR}/L_1 L_{TR\_i} L_2} + \frac{L_3 - 1}{G_{TR}G_D/L_1 L_{TR\_i} L_2}. \tag{24}$$

NF_i varies with the attenuation L_{TR} in each T/R module, and the result in displayed in Figure 9(a). $NF_0 = 3.054$ is the noise figure without T/R weighting. NF_i keeps nearly constant if L_{TR} is less than 10 dB. The noise figure of each branch increases rapidly when L_{TR} is higher than 15 dB.

Taylor weighting is applied in the elevation direction of the AESA. The attenuation values in T/R modules are shown in Figure 9(b) for sidelobe level (SLL) −25 dB, −35 dB, and −40 dB. For branches at both sides, the attenuation is larger than 10 dB.

The antenna array noise figure F_a is calculated by equation (12) and displayed in Table 2. We compare F_a with NF_0/ε_T. The difference is less than 0.1 dB even though some T/R modules are deeply attenuated. Thus, NF_0/ε_T is very practical in estimating the noise figure of an AESA.

4. Conclusion

In this paper, a practical and universal two-port model for the noise of an AESA is presented, and an example is of a SAR antenna is applied. From this model, an antenna array with a multistage combiner network is equivalent to a one-stage combiner network, and the calculation of the noise figure is greatly simplified. Besides, NF_0/ε_T can be used to estimate the noise figure of an AESA if the gain of LNA in T/R modules is sufficiently large. The noise model is expected to be useful in evaluating the SNR of receiving system with multichannel antenna arrays.

Data Availability

The data used to support the findings of the study are available upon request from the corresponding author.

Conflicts of Interest

The authors declare that they have no conflicts of interest.

References

[1] U. Kraft, "Gain and G/T of multielement receive antennas with active beamforming networks," *IEEE Transactions on Antennas and Propagation*, vol. 48, no. 12, pp. 1818–1829, 2000.

[2] J. J. Lee, "G/T and noise figure of active array antennas," *IEEE Transactions on Antennas and Propagation*, vol. 41, no. 2, pp. 241–244, 1993.

[3] R. V. Gatti, M. Dionigi, and R. Sorrentino, "Computation of gain, noise figure, and third-order intercept of active array antennas," *IEEE Transactions on Antennas and Propagation*, vol. 52, no. 11, pp. 3139–3142, 2004.

[4] J. Yun, J. Y. Park, and K. C. Hwang, "Optimization of a subarray structure to improve the G/T of an active array antenna," *IEEE Antennas and Wireless Propagation Letters*, vol. 18, no. 10, pp. 2214–2218, 2019.

[5] E. Holzman, "A different perspective on taper efficiency for array antennas," *IEEE Transactions on Antennas and Propagation*, vol. 51, no. 10, pp. 2963–2967, 2003.

[6] A. Kumar, D. Chaturvedi, and S. I. Rosaline, "Design of antenna-multiplexer for seamless on-body internet of medical things (IoMT) c," *IEEE Transactions on Circuits and Systems II: Express Briefs*, vol. 69, no. 8, pp. 3395–3399, 2022.

[7] D. Chaturvedi, A. Kumar, and S. Raghavan, "Wideband HMSIW-based slotted antenna for wireless fidelity application," *IET Microwaves, Antennas & Propagation*, vol. 13, no. 2, pp. 258–262, 2019.

[8] A. Ayman, "Design of half-mode substrate integrated cavity inspired dual-band antenna," *International Journal of RF and Microwave Computer-Aided Engineering*, vol. 31, Article ID e22520, 2021.

[9] R. J. Mailloux, *Phased Array Antenna Handbook*, Artech House, Norwood, MA, USA, 2 edition, 2005.

[10] D. Pozar, *Microwave Engineering*, Wiley, Hoboken, NJ, USA, 2005.

[11] R. Steven, "realized noise figure of the general receiving antenna," *IEEE Antennas and Wireless Propagation Letters*, vol. 12, pp. 702–705, 2013.

[12] Keysight Technologies, "Noise Figure Measurement Accuracy: The Y-Factor Method," 2001, https://www.keysight.com/cn/zh/assets/7018-06829/application-notes/5952-3706.pdf.

[13] Keysight Technologies, "Fundamentals of RF and Microwave Noise Figure Measurements," 1983, https://www.keysight.com/cn/zh/assets/7018-06829/application-notes/5952-8255.pdf.

[14] Q. Zhang and Y. Liu, "Overview of Chinese first C band multi-polarization SAR satellite GF-3," *Aerospace China*, vol. 18, no. 3, pp. 22–31, 2019.

[15] J. Sun, W. Yu, and Y. Deng, "The SAR payload design and performance for the GF-3 mission," *Sensors*, vol. 17, no. 10, p. 2419, 2017.

[16] J. Mi, H. Sun, G. Song, Y. Xing, and X. Zhao, "Realization of low cross-polarization level for GF-3 SAR antenna," *International Journal of Antennas and Propagation*, vol. 2022, 8 pages, Article ID 9260843, 2022.

[17] J. Mi, H. Sun, Y. Xing, X. Zhao, and J. Li, "SAR antenna pattern measurement by internal calibration method for GF-3 satellite," *International Journal of Antennas and Propagation*, vol. 2022, 9 pages, Article ID 5881971, 2022.